

A 3D electron microscopy segmentation pipeline for hyper-realistic diffusion simulations

Poster Number:

1342

Submission Type:

Abstract Submission

Authors:

Michiel Kleinnijenhuis¹, Errin Johnson², Jeroen Mollink^{1,3}, Saad Jbabdi¹, Karla Miller¹

Institutions:

¹Oxford Centre for Functional MRI of the Brain, University of Oxford, Oxford, United Kingdom, ²Sir William Dunn School of Pathology, University of Oxford, Oxford, United Kingdom, ³Department of Anatomy, Donders Institute for Brain, Cognition & Behaviour, Radboud University Medical Center, Nijmegen, Netherlands

Introduction:

The microstructural complexity of white matter (WM) is often not captured in diffusion MRI models. This can skew interpretations of the underpinnings of the MR signal. We aim to address this shortcoming by using hyper-realistic simulations based in microscopy data. Here, we present a pipeline for creating realistic mesh models from 3D electron microscopy. Additionally, we provide reference data for WM microstructure, in particular on myelination characteristics.

Methods:

Our pipeline (Figure 1A) was tested on serial blockface scanning electron microscopy (Denk, 2004) data (resolution 7.3x7.3x50 nm, FOV ~60x60x23 µm) acquired from the genu of a sagittal mouse corpus callosum section prepared according to Wilke (2013) with a Zeiss Merlin Compact Scanning Electron Microscope + Gatan 3View system.

The most essential components of the segmentation pipeline:

[1] Generating compartment probability maps by interactive pixel classification with Ilastik (Sommer, 2013).

[2] Labeling of myelinated axons (MA). Connected component labeling is performed slice-wise in 2D on an isotropically downsampled myelin mask created by thresholding the myelin probability map ($P > 0.2$). The 3D MA compartment is then generated by aggregating labels along the slice direction, where gaps are filled by an anisotropic closing operation (6 slices). Morphological image closing and hole-filling are performed to include mitochondria in the MA compartment. This stage is completed by manual editing to correct residual errors.

[3] Separating individual myelin sheaths (MM) by watershed of the distance transform of the MA mask. Only voxels extending no more than 0.25 µm from the MA mask are considered, which excludes mitochondria often included in the myelin mask.

[4] The remaining tissue compartments, mainly unmyelinated axons, are segmented by automated classification with Neuroproof (Parag, 2015). First, supervoxels are generated by watershed of the probability map for intracellular space. Next, a random forest classifier is trained on a semi-manually annotated training dataset. Finally, the supervoxels are agglomerated to form the processes of unmyelinated axons (UA), glial processes (GP) / bodies (GB) and blood vessels (BV). This stage also requires proofreading to correct split/merge errors.

A) Pipeline flow chart. Black text indicates the outcome of each step, while orange text represents the method used.

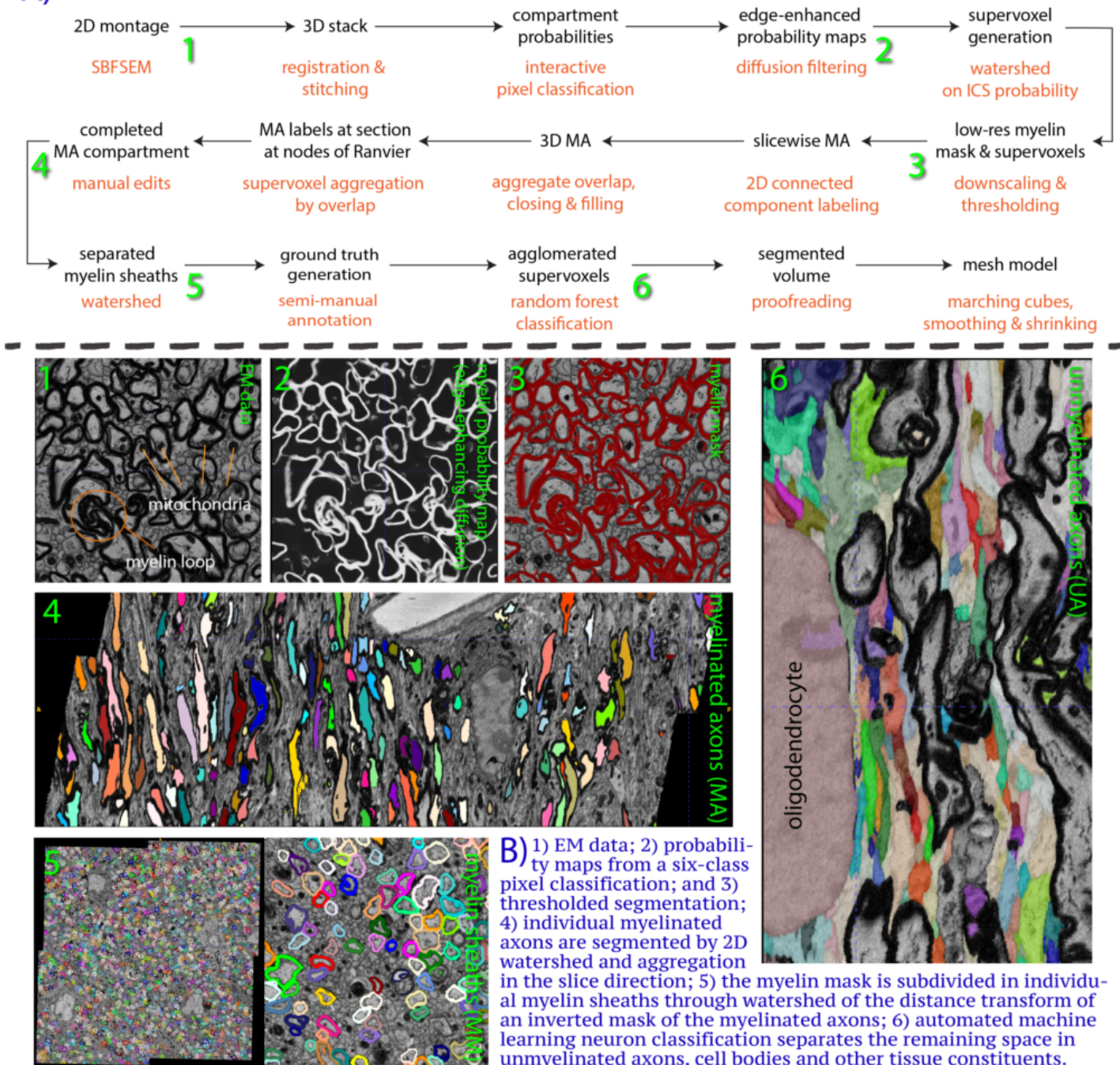


Figure 1. Segmentation pipeline. A) Pipeline flow chart; B) Segmentation results.

Results:

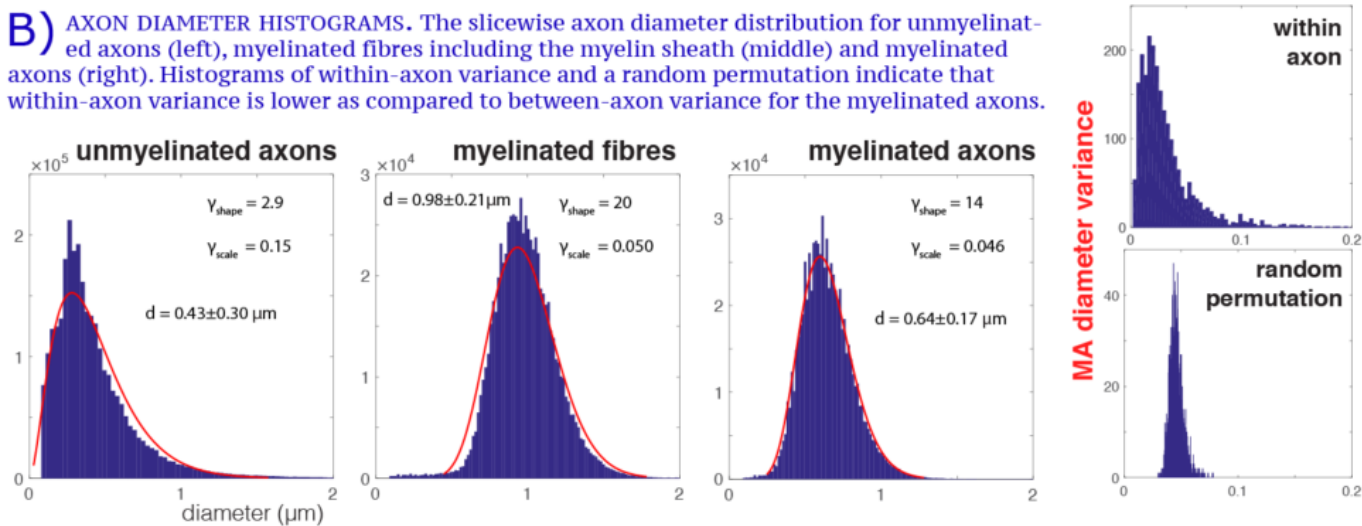
Myelinated axons and myelin sheaths were sufficiently large to be reliably segmented at an isotropic resolution of 50 nm (Figure 1B), greatly facilitating computation and manual editing speed (~40h for this dataset). Sheaths are accurately separated where the geometry is simple, but the automated segmentation fails in locations where oligodendrocyte processes form loops. The machine learning method of neuron classification has residual errors where cellular processes are erroneously split or merged. However, it is sufficient for our purpose, as it does capture the structure and compartment size of the tissue.

A summary of tissue properties derived from the segmentation is provided in Figure 2. The average g-ratio was lower than expected (West, 2015). The within-axon variance of axon diameter was found to be larger than the between-axon variance. A near-linear correlation was observed between the g-ratio and axon diameter.

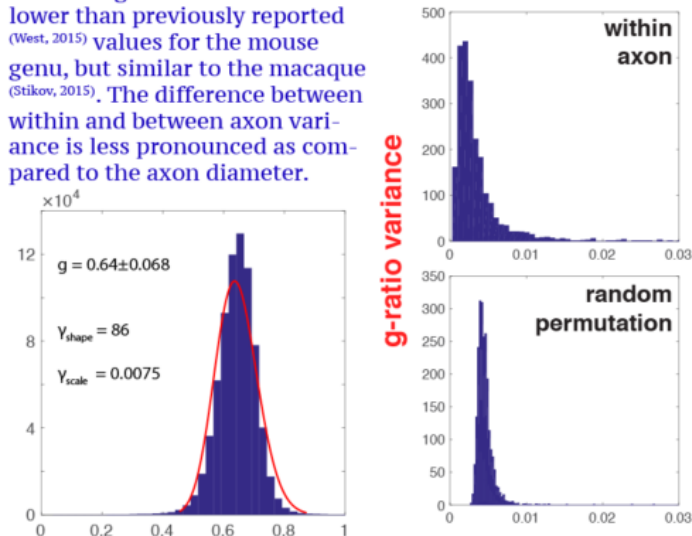
A) COUNTS AND VOLUMES. The axon diameter is given as mean±std. The rather high standard deviation for the unmyelinated axons is presumably due erroneous merging of axons by the automated neuron classification, or the inclusion of the larger glial processes in this compartment. MA=myelinated axons, MM=myelin, UA=unmyelinated axons, GL=glia, BV= blood vessel. The glial bodies and major processes and the blood vessel are grouped together in the volume statistic.

	MA	MM	UA	GL	BV
count	2280	2280	27778	10	1
volume (µm³)	12992	16898	30268	7383	
volume fraction	.19	.25	.45	.11	
mean diameter* (µm)	.64±.17	.98±.21	.43±.30		

B) AXON DIAMETER HISTOGRAMS. The slicewise axon diameter distribution for unmyelinated axons (left), myelinated fibres including the myelin sheath (middle) and myelinated axons (right). Histograms of within-axon variance and a random permutation indicate that within-axon variance is lower as compared to between-axon variance for the myelinated axons.



C) G-RATIO HISTOGRAMS. The g-ratio was somewhat lower than previously reported (West, 2015) values for the mouse genu, but similar to the macaque (Stikov, 2015). The difference between within and between axon variance is less pronounced as compared to the axon diameter.



D) AXON DIAMETER VS. G-RATIO. The relation between axon diameter and g-ratio appears non-linear (West, 2015; Stikov, 2015).

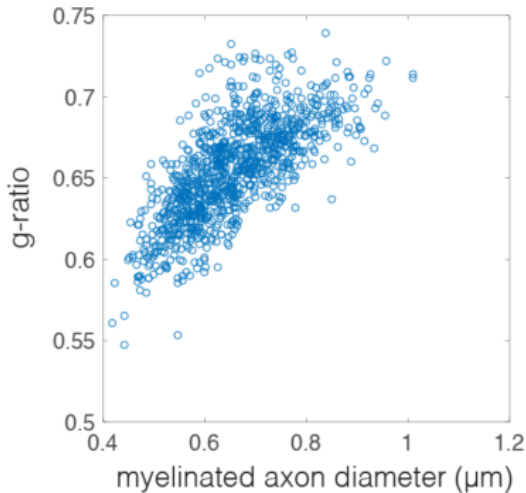


Figure 2. Compartment properties. A) counts and volumes; B) axon diameter histograms; C) g-ratio histograms; D) axon diameter vs. g-ratio scatter plot.

Conclusions:

We have developed a method for segmenting large 3D electron microscopy datasets of WM requiring minimal intervention. While existing algorithms focus on grey matter, we provide a method that segments individual myelin sheaths, cell processes and bodies. Our approach can easily incorporate additional compartments such as mitochondria. The 2D myelin segmentation has the benefit that nodes of Ranvier are automatically annotated. Complex myelin wrappings (Figure 1B.1) remain a difficulty, as they are not easily assigned to a single axon. Apart from paving the way for hyper-realistic diffusion MRI simulations, our models provide informative benchmark statistics of WM microstructure and robust quantification method for subtle differences in myelination.

Imaging Methods:

Diffusion MRI
Imaging Methods Other

Modeling and Analysis Methods:

Diffusion MRI Modeling and Analysis ¹
Methods Development

Neuroanatomy:

White Matter Anatomy, Fiber Pathways and Connectivity ²

Keywords:

Cellular
Demyelinating
Glia
Machine Learning
Modeling
MRI PHYSICS
Myelin
Segmentation
White Matter
Other - electron microscopy

^{1|2}Indicates the priority used for review

Would you accept an oral presentation if your abstract is selected for an oral session?

Yes

I would be willing to discuss my abstract with members of the press should my abstract be marked newsworthy:

Yes

Please indicate below if your study was a "resting state" or "task-activation" study.

Other

By submitting your proposal, you grant permission for the Organization for Human Brain Mapping (OHBM) to distribute the presentation in any format, including video, audio print and electronic text through OHBM OnDemand, social media channels or other electronic media and on the OHBM website.

I accept

Healthy subjects only or patients (note that patient studies may also involve healthy subjects):

Healthy subjects

Internal Review Board (IRB) or Animal Use and Care Committee (AUCC) Approval. Please indicate approval below. Please note: Failure to have IRB or AUCC approval, if applicable will lead to automatic rejection of abstract.

Not applicable

Please indicate which methods were used in your research:

Other, Please specify - electron microscopy

Which processing packages did you use for your study?

Other, Please list - Ilastik, ITK-SNAP, Neuroproof, scikit-image

Provide references in author date format

Denk, W. (2004), 'Serial block-face scanning electron microscopy to reconstruct three-dimensional tissue nanostructure', PLoS Biology vol. 2, pp. e329
 Wilke, S.A. (2013), 'Deconstructing complexity: serial block-face electron microscopic analysis of the hippocampal mossy fiber synapse', The Journal of Neuroscience vol. 33, no. 2, pp.507-522
 Sommer, C. (2011), 'Ilastik: Interactive Learning and Segmentation Toolkit', Eighth IEEE International Symposium on Biomedical Imaging (ISBI) Proceedings, pp. 230-233
 Parag, T. (2015), 'A Context-Aware Delayed Agglomeration Framework for Electron Microscopy Segmentation', PLoS ONE 2015, vol. 10, no. 5, pp. e0125825
 West, K.L. (2015), 'Quantitative analysis of mouse corpus callosum from electron microscopy images', Data in Brief, vol. 5, pp. 124-128
 Stikov, N. (2015), 'In vivo histology of the myelin g-ratio with magnetic resonance imaging', Neuroimage, vol. 118, pp. 397-405

